CHAPTER-4

RESULTS AND DISCUSSION

CHAPTER-4

RESULTS AND DISCUSSION

All video recordings at 120 fps (frame per second) and 400 fps were analysed using image processing algorithms discussed in the previous section. From these recordings, gas holdup, ε, structure of the bed, bubble size distribution (BSD), Sauter-mean bubble diameter, d_b, aspect ratio, E, and specific interfacial area of bubbles, a_i, were estimated. The findings are presented in this chapter. The effect of static bed height and superficial gas velocity ~~studied~~ on BSD, d_b and a_i, were studied. The effect of physical properties of the liquid was studied by comparing results for water with CMC solution of various concentrations.

4.1 Structure of the Bed

The studies on structure of the bubble column included identification of expanded column height, its dynamic behaviour, measurement of foam layer thickness and the thickness of entry layer near the sparger. The video for this purpose was recorded at 120 fps.

A typical frame for such recording (equivalent to a gap of 0.00833 s) is shown in Figure 4.1a. Visual observation of the bubble column had indicated the presence of a foam layer at the top with few bubble burst resulting in entrainment of the liquid above the air-water dispersion. Due to rapid variation of bed height it was not possible to measure the foam layer manually. It was even more difficult in the case of entry region.

4.1.1 Pixel density in vertical direction

The image after applying a series of image processing methods was converted to binary image containing only white and black pixels as shown in Figure 4.1b. The white pixels corresponding to gas have the value 1 and the black pixels corresponding to water have the value 0. The pixel density at any height above the distributor plate, H, is defined as ratio of sum of all pixel values to the number of pixels at H. Variation of pixel density as a function of height above the distributor plate for superficial gas velocity, U_g, = 0.105 m.s^{-1} and static bed height, H_s = 0.145 m (corresponding to the image in Figure 4.1a) is shown in Figure 4.1c. Figure 4.1a, 4.1b and 4.1c are on the same scale. Bottom of the binary image corresponds to the region adjacent to the sparger. The top of the image is black due to absence of liquid. Presence of small isolated value of pixel density at a height, H = 0.37 m is attributed to entrainment of liquid after bursting of air bubble. The top surface of the bed was not horizontal. The height at which last peak observed in Figure 4.1c was taken as the value of average expanded bed height, H_e, in each frame.

Variation of pixel density with H is not smooth. It shows an increasing trend above the sparger and in most of the video-frames there is a distinct drop in pixel density at about H=0.4 m. On comparison with the image (Figure 4.1a) it was decided to take this height as the thickness of the entry region. At the bottom of the column, value of pixel intensity is very less. It is due to the presence of large number of bubbles at the bottom of the column i.e. near the sparger. The pixel density shows an increasing trend with increasing value of H. Near the top at about H=0.22 m a sudden drop in pixel density was observed. It again increases, passes through a maximum value and decreases. It was observed in all the cases and was attributed to the presence of a foam

layer after comparing with the image. In some cases a small peak again appears. It was due to bursting of bubble and was included while estimating the expanded bed height.

4.1.2 Fluctuating nature of liquid layer

Few typical examples of fluctuation of expanded bed height, H_e, with time is shown in Figure 4.2. The value of H_e were obtained from each graphs as shown in Figure 4.1c for each successive frame of video. The fluctuations in H_e are rapid and suggest its cyclic variation of with time.

To understand the effect of superficial gas velocity, U_g on H_e, variation of pixel density along the height of the column at H_s =0.15 m for three values of U_g = 0.042, 0.084 and 0.168 m.s^{-1} are presented in Figure 4.3a through 4.3c. The trend for all values of U_g is similar to that presented in Figure 4.1c. The increase in pixel density in lower portion of the column is gradual. The decrease in pixel density at $H > 0.15$ m becomes less sharp with increasing U_g. Beyond the expanded bed height, H_e, i.e. at $H > H_e$, the pixel density drops to a very small value showing absence of any bubbles. At this location average liquid layer was taken to exist. In all these cases, the difficulty in identifying presence of entry layer may be observed.

To observe effect of U_g and H_s on the fluctuations of H_e with time, few more cases are presented in Figure 4.4. At U_g = 0.042 m.s^{-1} the fluctuations were small at all three values of H_e. At high gas velocity, U_g = 0.084 m.s^{-1} large rapid fluctuations (> 10 per second) were observed.

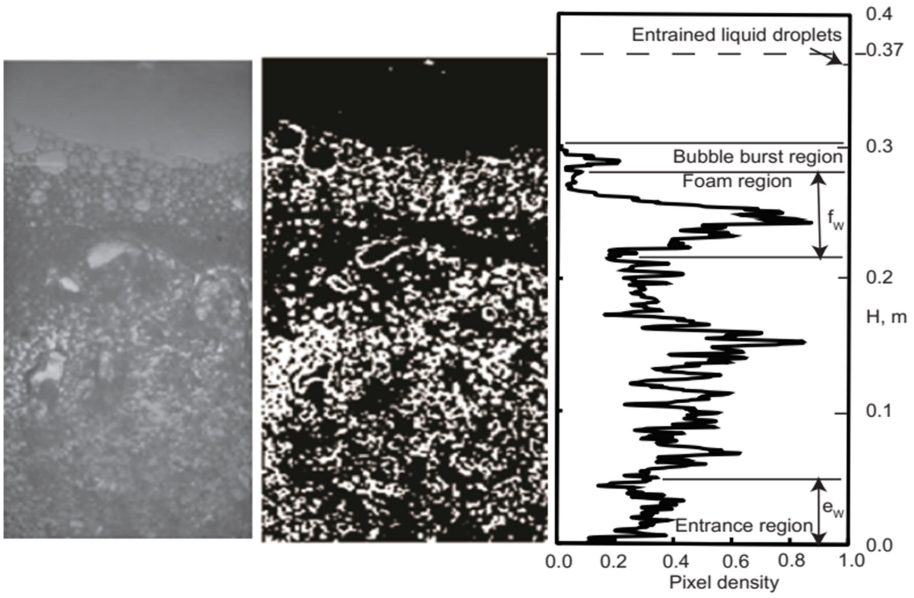

Figure 4.1 Image of air-water dispersion in bubble column (a) on left-original image (b) in middle-final binary image (c) on right-Pixel density at different position above distributor plate

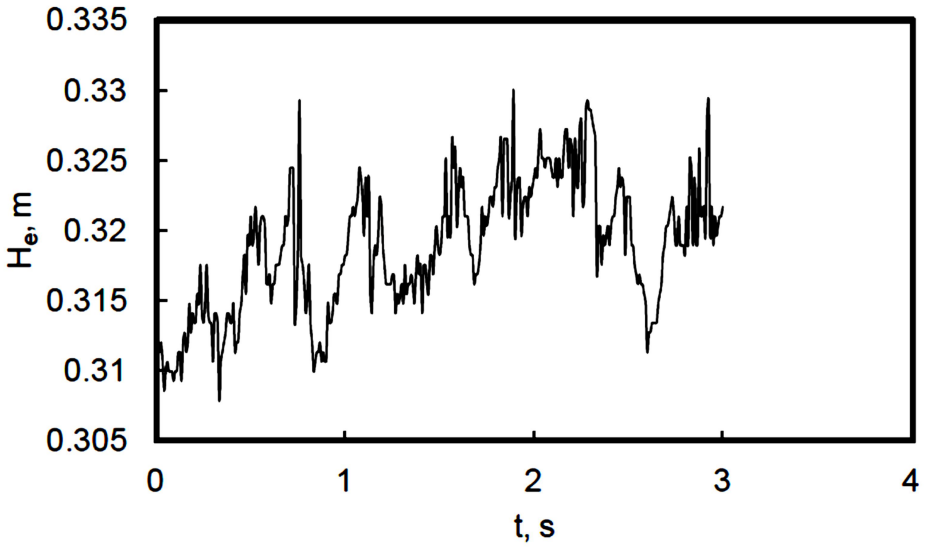

Figure 4.2 Variation of H_e with time at different U_g and H_s for air water system

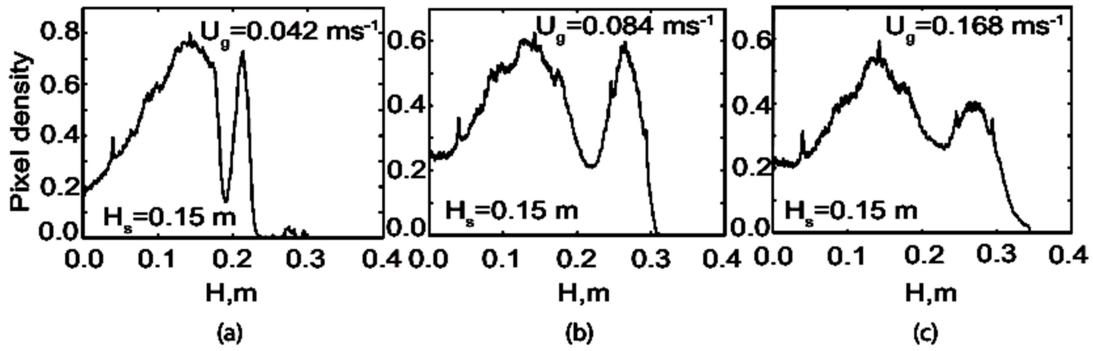

Figure 4.3Effect of U_g on pixel density as a function of H at (a) U_g = 0.042 m.s^{-1} (b) U_g = 0.084 m.s^{-1} (c) U_g = 0.168 m.s^{-1}

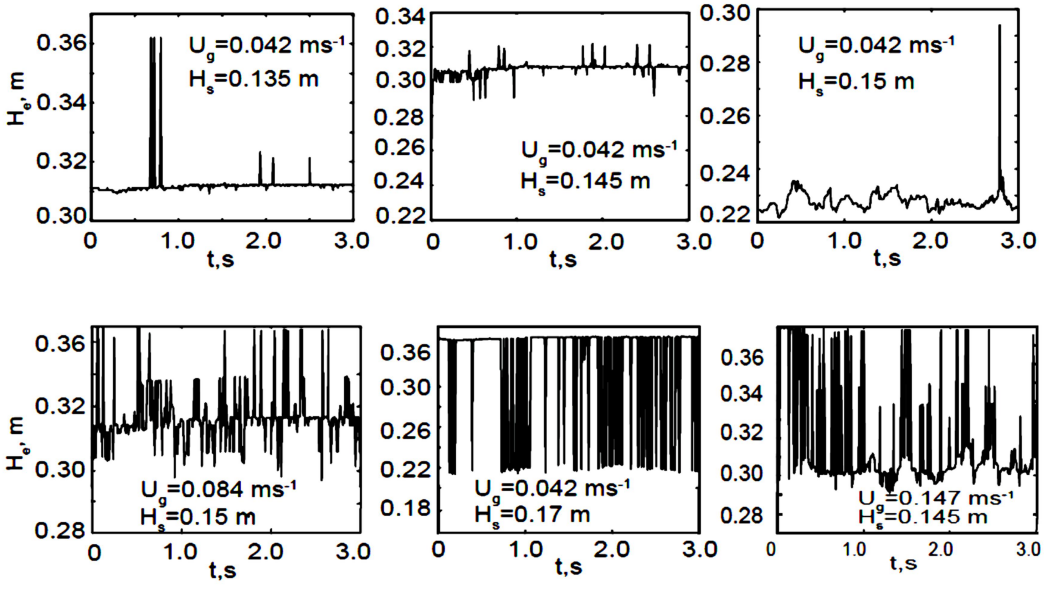

Figure 4.4: Variation of H_e with time at different U_g and H_s for air water system

The study the nature of fluctuations of liquid layer, autocorrelation function (ACF) from H_e vs t time-series was determined. Few typical values are presented in Figure 4.5. Cyclic nature is more prominent at high values of H_s or U_g. Auto correlation for bubble flow displays both bubble growth and acceleration. When bubble growth in the column is too fast, then soon there will be a bubble coalescence and bubble breakup. Two peaks are formed at 0.75 sec and 1.5 sec. These peaks give information about the breakup of large bubbles at the surface of liquid. Break-up occurs when the inertial forces acting on the bubble which try to deform the bubble are larger than the surface force which tries to keep it in shape as one single bubble. The ACF was estimated as

$$ACF = \sum_{all\ \Delta t} H_e(t).H_e\left(t-\Delta t\right).$$

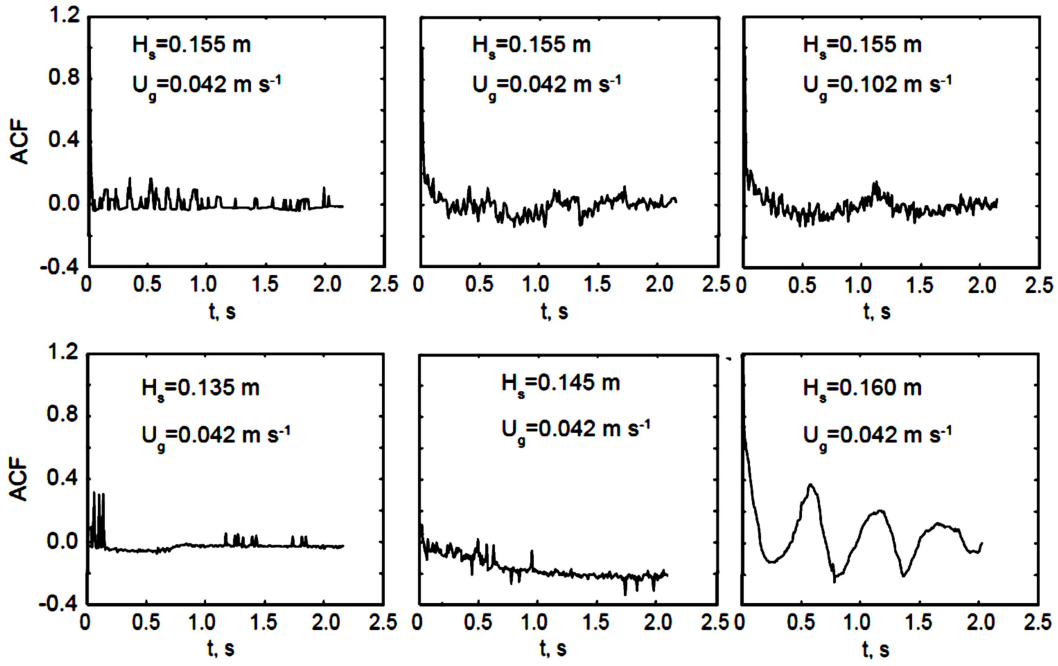

Figure 4.5: Variation of ACF with time at different U_g and H_s for air water system

To study the periodicity of the fluctuations in expanded bed height autocorrelation coefficient of time series of H_e were estimated. Indirectly it also indicated the periodicity in gas holdup vs time. The auto-correlation coefficient (*ACF*), is a measure of periodic variation. The variation of ACF with time for U_g = 0.168 m.s^{-1} and H_s = 0.145 m is presented in Figure 4.6. The periodic variation with time period of about 0.8 s can easily be seen from the figure. It can be attributed to the presence of large bubbles which are formed by bubble coalescence in the column. The changes in ACF may be useful to identify the flow regime.

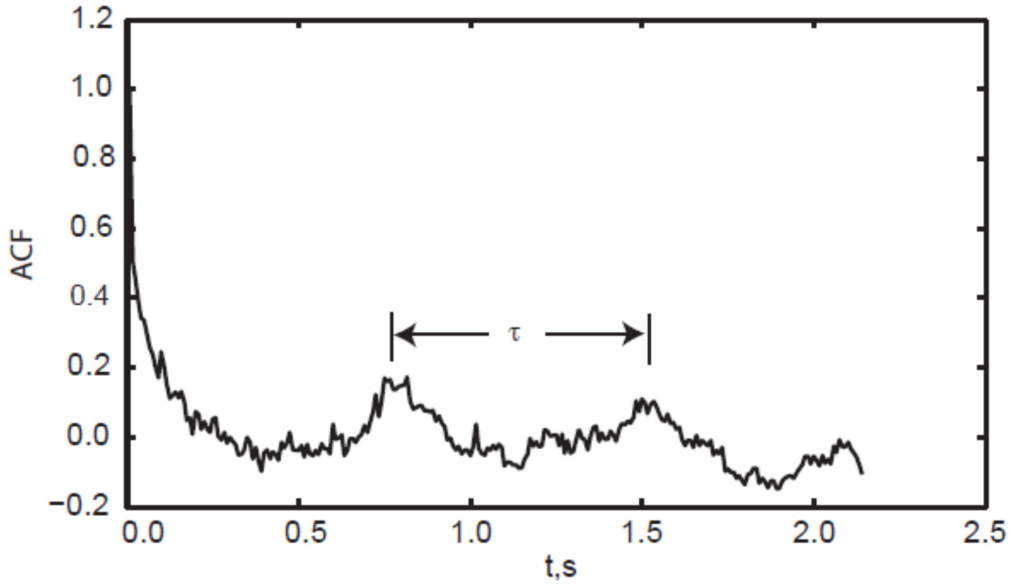

Figure 4.6: *ACF* vs time for U_g = 0.168 m.s^{-1} and H_s = 0.145 m

Time period of periodic variation of H_e were estimated and are plotted as a function of U_g and H_s is presented in Figure 4.7. There was no noticeable periodic variation of expanded bed height for U_g < 0.08 m.s^{-1}. Therefore, no data could be obtained from ACP. At all values of H_s the time period shows a maximum value for the value of U_g in the range of 0.11-0.15 m.s^{-1}. It may be attributed to change of flow regime from homogeneous to churn-turbulent flow regime. The effect of H_s on the time period is not very clear suggesting a weak dependence if any.

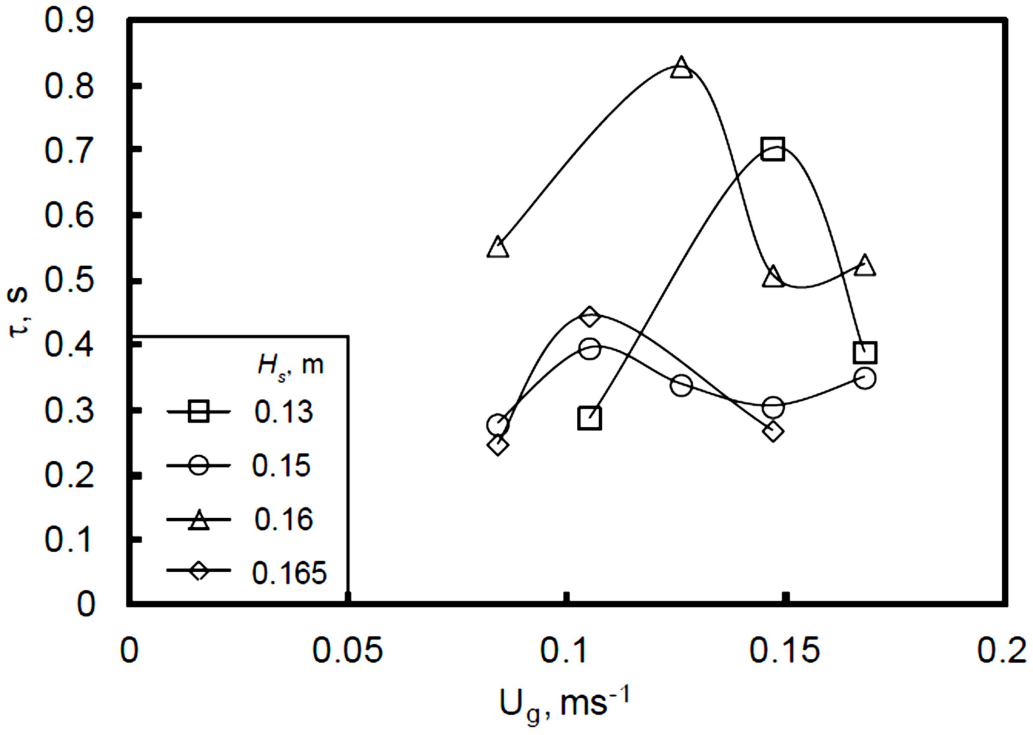

Figure 4.7: τ vs U_g as a function of H_s

4.1.3 Foam layer thickness

The foam layer width, f_w, was estimated from graphs of pixel density as a function of H_s for 60 successive frames (corresponds to 0.5 s). Average values of f_w are reported in this study. Present values of f_w at H_s = 0.135 m as a function of U_g are compared with correlations of Yamashita [1995] and Pilon et al. [2001] in Figure 4.8.

Yamashita (1995) proposed following correlation for f_w.

$$f_W = 15U_g^{0.73} \tag{4.1}$$

Pilon et al. [2001] proposed following correlation for f_w in case of highly viscous liquids.

$$f_W = 2905(d_b / 2)Ca^{-1}\left(Fr'/Re\right)^{1.8} \tag{4.2}$$

Dimensionless numbers, Capillary number, *Ca*, Froude number, *Fr*, and Reynolds number, *Re,* were defined as

$$Re = \rho_l(d_b / 2)\left(U_g - U_{gf}\right)/\mu_l \tag{4.3a}$$

$$Fr' = \left(U_g - U_{gf}\right)^2/(gd_b / 2) \tag{4.3b}$$

$$Ca = \mu_l\left(U_g - U_{gf}\right)/\sigma_l \tag{4.3c}$$

Here, U_{gf} is the gas velocity at onset of foaming, conditions for which in case of pneumatic foams were reported in a later study [Pilon and Viskanta (2004)]. The value of U_{gf} can easily be obtained by extrapolating the data for f_W vs U_g (see Figure 4.8) and can be used in Equation 4.2.

While using Equation 4.2, the gas velocity at which onset of foaming occurs was determined by fitting the present data by a second order polynomial and

extrapolating it to the x-axis where $f_w = 0$. The extrapolation is shown by the dotted line. The value of bubble diameter was taken as 0.004 m as measured from photographically. The value of U_{gf} thus estimated is 0.0064 m.s^{-1}. Both correlations show monotonically increasing value of f_w. At U_g= 0.042 m.s^{-1} the present value is in close agreement to the values predicted by both correlations. The methodology developed to measure the foam layer thickness is thus validated. The values of f_w estimated from Equations 4.2 and 4.3 increased to 0.118 m and 0.132 m respectively at U_g = 0.168 m.s^{-1}. In the present study it showed a maximum value of 0.061 m at U_g = 0.126 m.s^{-1}. The deviation at higher gas velocity may be due to the change in bubble diameter. The foam layer thickness is known to be very sensitive to the bubble radius [Pilon and Viskanta (2004)].

The values of f_w as a function of U_g and H_s are presented in Figure 4.9. The foam width increases with increasing U_g upto a value of U_g = 0.1 m.s^{-1} above which it starts decreasing. This trend was observed at all values of H_s. The effect became less prominent as the value of H_s increased. This trend is not in accordance with the results of Yamashita [1995] who found that the foam layer thickness increases monotonically with increasing gas velocity. The maximum foam width decreased with increasing value of H_s. Yamashita [1995] measured foam layer thickness for H_s in the range of 0.5 m – 0.79 m, which is almost double as compared to the value H_s used in the present study. It indicates that the foam layer thickness may not follow monotonic increasing trend at low values of H_s.

The gas velocity at which maximum foam thickness is same as the velocity upto which uniform bubbling occurs i.e. upto U_g < 0.1 m.s^{-1}. During transition from uniformly bubbly regime to churn turbulent regime the foam layer thickness decreases. Present experimental conditions did not cover a wide range of churn-turbulent conditions. As only small bubbles are present at low U_g, the bubbles do not get

sufficient time for coalescence to take place and leave the column before it could happen. Hence. at low velocities the foam layer thickness increases with U_g.

At large values of U_g bubble coalescence takes place. It results in formation of large bubbles which move at large velocity and burst at the top. As a result the foam layer decreases. At high values of H_s, bubbles get sufficient time coalesce. Hence number of large bubbles reaches at the top increases, they break easily due to being less stable. Thus, foam formation at the top is reduces with increasing H_s. The present data is at low value of H_s and hence the present trend is applicable to shallow beds only.

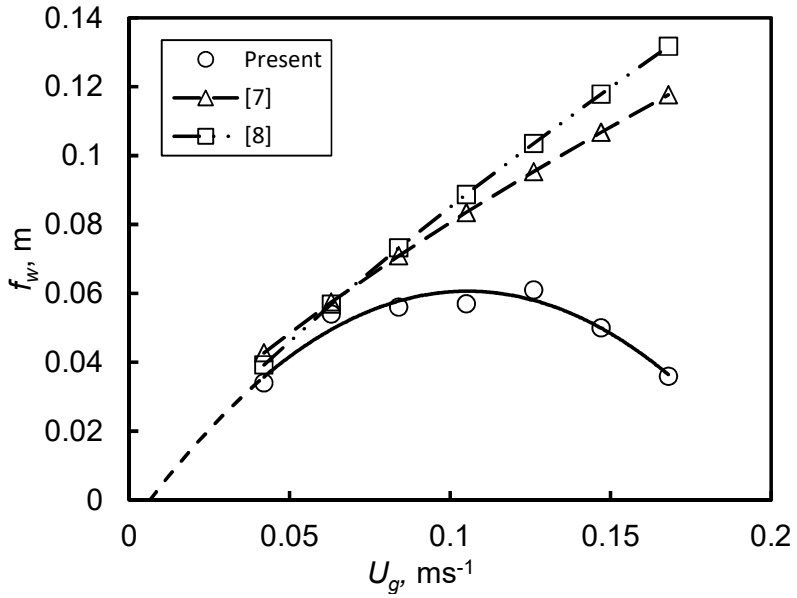

Figure 4.8 Comparison of f_w with correlations of Yamashita (1995) and Pilon et al.(2001).

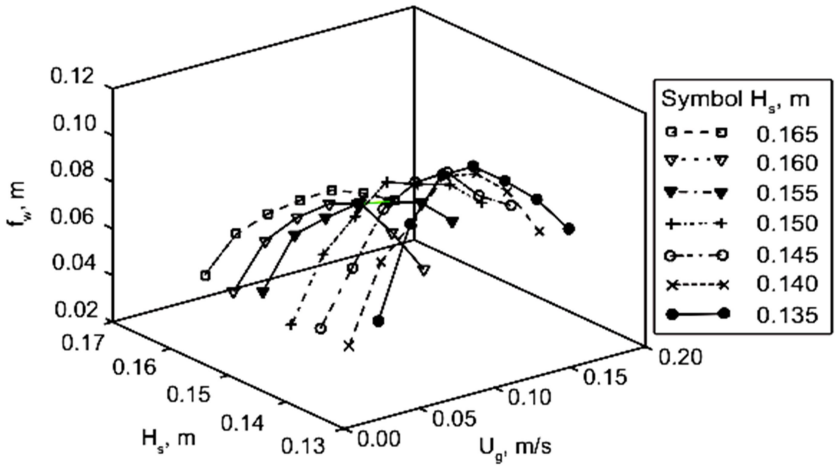

Figure 4.9 f_w as a function of U_g and H_s

4.1.4 Entry Region Width

The entry region width, e_w, was estimated from pixel density as an average over 60 frames. Variation of e_w with H_s and U_g is presented in Figure 4.10. The width of entry region increases with increasing settled bed height. It increases upto U_g = 0.084 ms^{-1}. Above this value at low values of H_s, the value of e_w remains constant. It decreases at large value of U_g. The trend is same at all values of H_s. The present trends do not follow monotonic increase of entrance layer as predicted by Equation 4.2 [Yamashita (1995)].

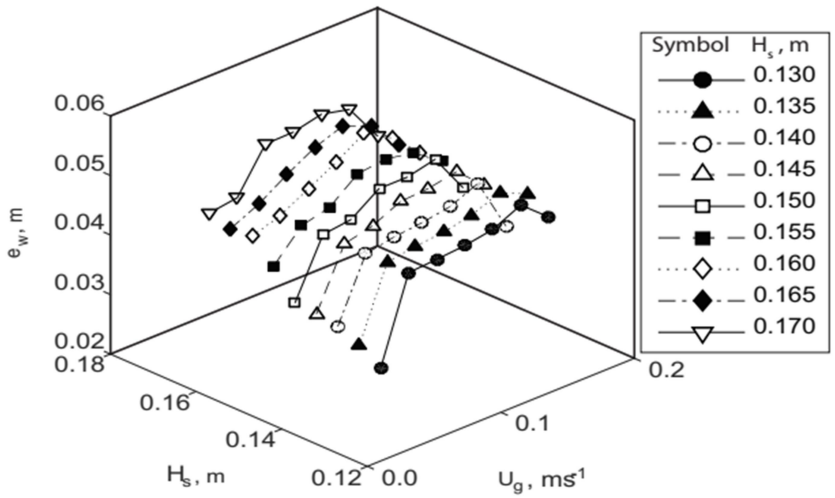

Figure 4.10: e_w as a function of U_g and H_s

4.2 Gas Holdup

For the measurement of ε, BSD, d_b and a_i video was recorded at 400 fps. Gas holdup has been widely studied. In the present study the gas holdup was estimated using the following expression.

$$\varepsilon = \frac{V_G}{V_G + V_L} \tag{4.4}$$

Here V_G and V_L are volume of gas and liquid phases in the column respectively. The bubbles diameter and shape of bubbles were determined using 'regionprops' function of MATLAB. The image was cleaned by the method discussed in the previous chapter, before applying 'regionprops' method. The volume of the gas (air) was estimated by summing volume of all bubbles in the column.

$$V_G = \sum_{N_b} \frac{1}{6} f_{b,i} \left(\pi d_{b,i}^3 \right) \tag{4.5}$$

where $f_{b,i}$ is the number of i th class of bubbles, $d_{b.i}$ having bubble diameter d_b. The volume of liquid is estimated in terms of H_s and cross sectional area of the column, A_c.

$$V_L = H_s A_c \tag{4.6}$$

The gas holdup was also measured from pixel density in the expanded bed region by using the following equation.

$$\varepsilon_{pixel} = \frac{\text{Pixels occupied by bubbles}}{\text{Total pixels}} \tag{4.7}$$

The presence of pixel was considered as occurrence of the gas. Its absence was considered to represent liquid. To validate the concept, total pixel density in the region upto a height of H_e was compared with gas holdup estimated using Equation 4.4. A comparison between ε_{pixel} and ε is presented in Figure 4.11. At lower values both values are in close agreement. In this region, either overlapping bubbles were absent or the number of overlapping bubbles was insignificant. At high gas velocity, the gas holdup is high and the number of overlapping bubbles is significant. Therefore, ε_{pixel}, was lower than ε_g. In the region of overlapping bubbles, the error in estimation is about 10 %. Since the specific interfacial is proportional to gas holdup, gas holdup estimated by Equation. 4.4 was reported.

The values as a function of U_g for H_s in the range of 0.20 to 0.28 m for air-water system are presented in Figure 4.12. The gas holdup was estimated by taking the value of H_e averaged over all frame (360 frames) for 3 s. The value of ε increase with increasing value of $U_{g.}$ No effect of H_s on gas holdup is observed upto U_g =0.04 $m.s^{-1}$. Above this value of U_g large difference of ε at various values of H_s can be seen, however no definite trend could be observed. It may be attributed to flow regime transition from homogeneous glow regime to churn-turbulent design.

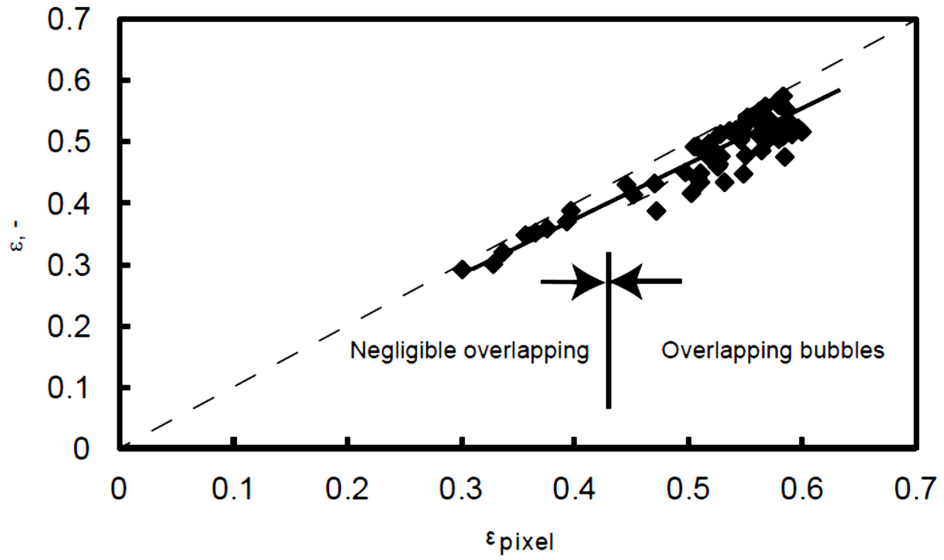

Figure 4.11: Correlation between gas holdup calculated by height measurement and pixel intensity

.

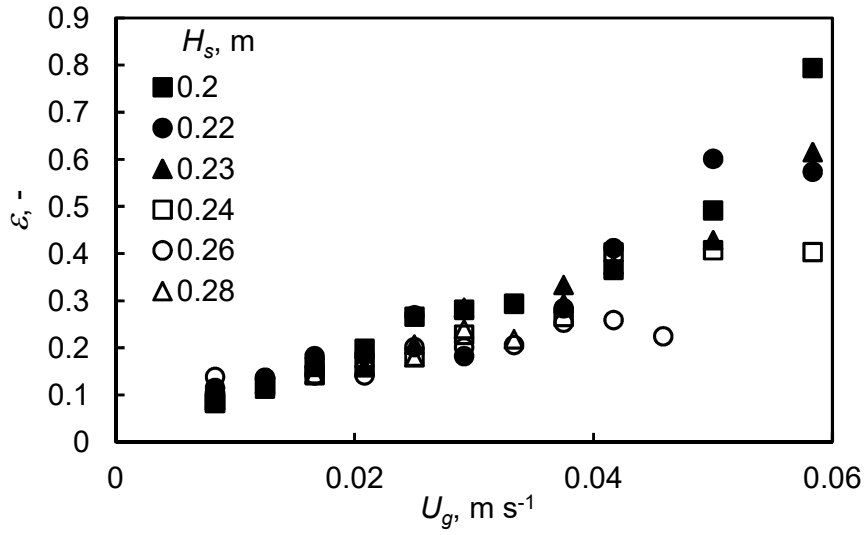

Figure 4.12: Variation of ε with U_g at H_s = 0.20 to 0.28 m for air water system

Drift flux diagram is used to know the fluid velocity at which the flow regime transition changes. A plot of U_g (1-ε) vs U_g at H_s = 0.20 to 0.28 m is presented in Figure 4.13. It can be seen that at U_g=0.04 m s^{-1} there is a change of slope for all values of H_s. confirming change of flow regime at U_g =0.04 m.s^{-1}.

4.2.1. Gas holdup for air-CMC solution system

Gas holdup as a function of U_g at H_s= 0.2 m for CMC conc. =0.5, 1.0, 2.0, and 3.0 % (w/w) for air-CMC solution are presented in Figure 4.14. The values of ε varies monotonically with U_g. The variation is smooth upto U_g =0.03 m.s^{-1}. Above this value of U_g gas holdup at CMC conc. = 3.0 % (w/w) suddenly increases. No significant effect of CMC conc. on U_g is observed below this value of U_g = 0.03 m.s^{-1}. It may be attributed to change of flow regime. The values of ε are lower than that observed for air-water system upto U_g =0.03 m.s^{-1}.

Drift flux plot (U_g (1-ε) vs U_g) at H_s = 0.20 m for CMC conc. =0.5, 1.0, 2.0, and 3.0 % (w/w) is presented in Figure 4.15. It can now be seen that the flow regime transition is at U_g =0.03 m.s^{-1}.

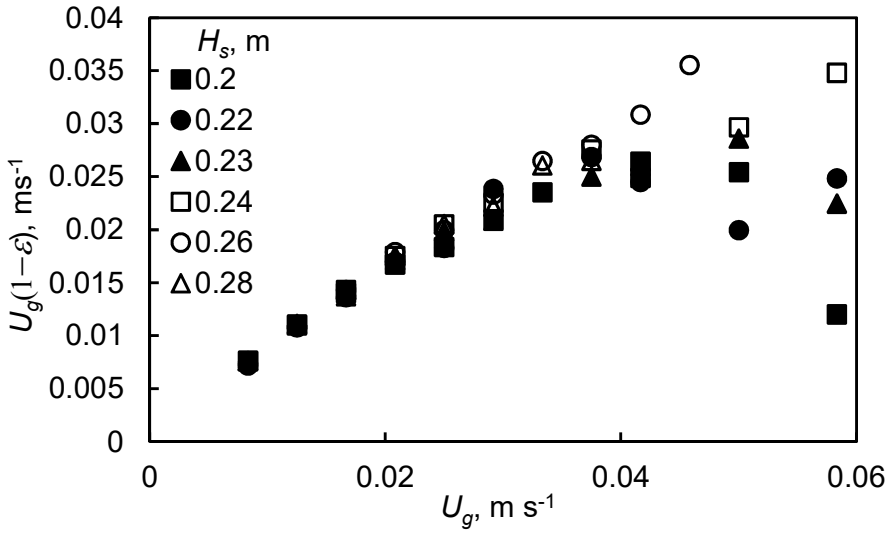

Figure 4.13: Drift flux diagram- U_g (1-ε) vs U_g at H_s = 0.20 to 0.28 m for air water system

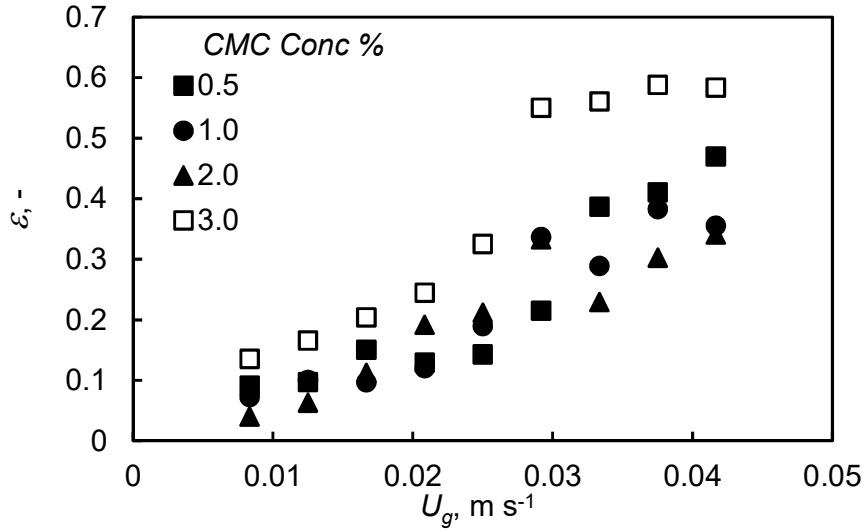

Figure 4.14: Variation of ε with U_g at H_s = 0.2 m for air-CMC soln. system at CMC conc. = 0.5, 1.0, 2.0 and 3.0 % (w/w).

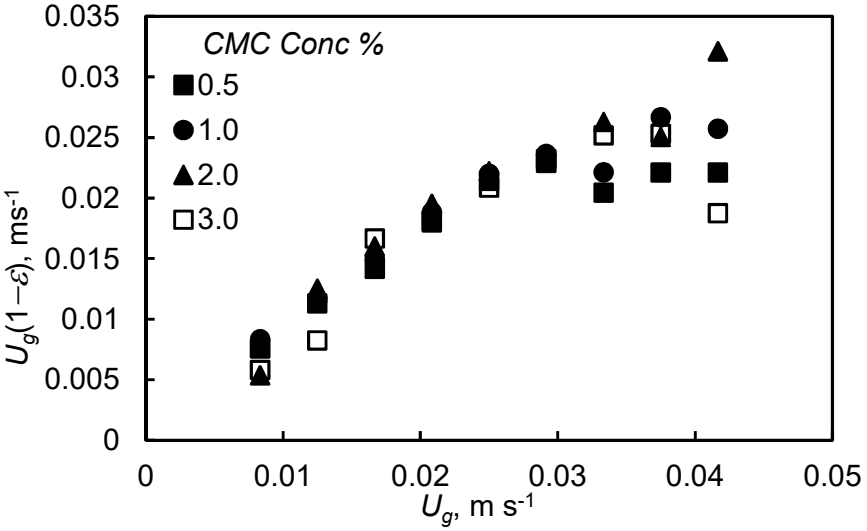

Figure 4.15: Drift flux diagram- U_g (1-ε) vs U_g at H_s = 0.2 m for air-CMC soln. system

4.3 Bubble Size Distribution (BSD)

Bubble size and shape were measured from a single frame of the movie. Bubble size distribution and Sauter-mean bubble diameter, d_{32}, based on number of bubbles counted in a frame were determined. Bubble shape was expressed as aspect ratio, E, defined as ratio of major axis to minor axis of ellipse. Specific interfacial area, a_i, was estimated from d_{32}.

4.3.1 BSD for Distilled Water

BSD for distilled water at superficial air velocity, U_g = 0.0416 m.s^{-1} and static bed height, H_s = 0.23 m is presented in Figure 4.16. It was difficult to measure bubbles of diameter less than 0.002 m. Number of bubbles, N_b, decreases smoothly with increasing d_b. It is a single model function. It can be observed that most of the bubbles are of the size about 0.002 m to 0.006 m, though few large bubbles may also be observed. Thus, it is not the case of uniform bubbling. It may be termed as non-uniform homogeneous flow regime or transition to churn-turbulent regime. The entire data of BSD for air-water system is presented in Tables A1 to A6 (Appendix-I).

4.3.1.1 Effect of U_g

BSD at H_s = 0.23 m, and for 0.008 m s^{-1} $\leq U_g \leq$ 0.058 m.s^{-1} is presented in Figure 4.17 to exhibit the dependence of U_g on BSD. It clearly shows that the bubbles formed are not of equal size. The sparger used in the present study did not have nozzles or holes of same size. It was constructed by placing glass beads on perforated plate and with a top of wire mesh. The striking feature is that the bubble size distribution is unaffected by the superficial gas velocity. There are large number of small bubbles having d_b=0.002 m. Number of bubbles smoothly decreases with increasing bubble diameter. Largest number having value of d_b=0.002 m decreases with increasing value of U_g.

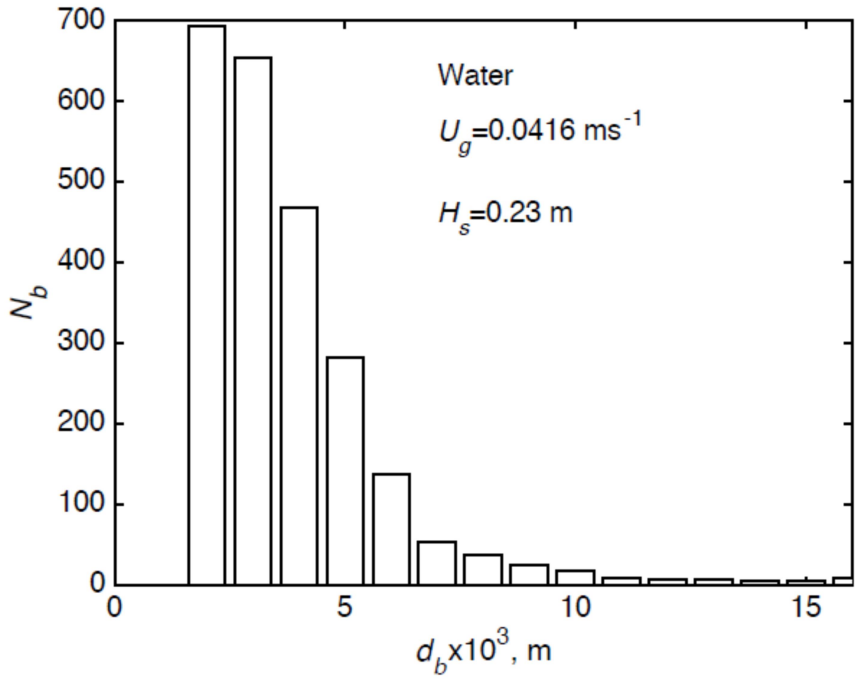

Figure 4.16: BSD for distilled water at U_g = 0.0416 m.s^{-1}, H_s = 0.23 m.

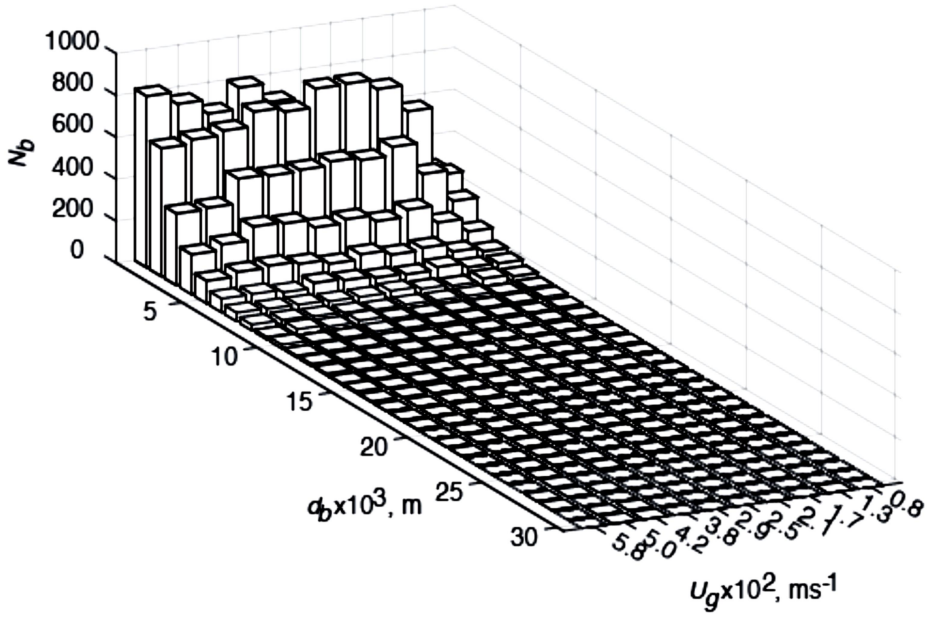

Figure 4.17: Effect of U_g on BSD for air-water at H_s = 0.23 m

The nature of BSD could have been fitted with log-normal distribution in such cases as reported in literature [Al-Masry et al (2007)]. However, it does not give a correct picture of occasionally large bubbles at higher gas velocity.

4.3.1.2 Effect of H_s

BSD at U_g=0.0167 m.s^{-1} for 0.20 m $\leq H_s \leq$ 0.28 m is presented in Figure 4.18. The BSD is similar at all values of H_s. The number of small bubbles seems to increase slightly with increasing H_s.

BSD at U_g=0.0417 m.s^{-1} for 0.20 m $\leq H_s \leq$ 0.26 m is presented in Figure 4.19. The trend is similar to that observed in Figure 4.17. Thus, only a small effect of H_s on BSD at all air velocity may be observed.

From the above observation it may be said that very few large bubbles were present for air-water system.

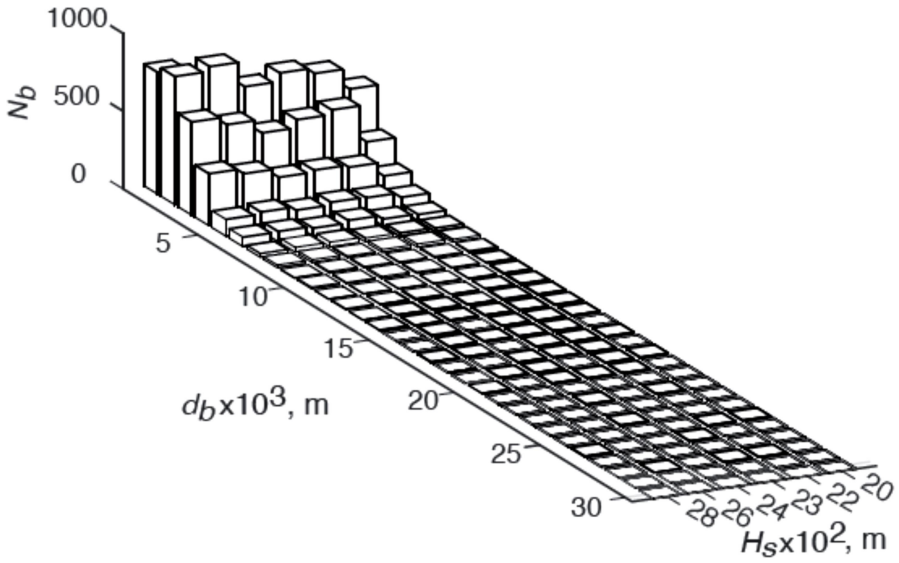

Figure 4.18: Effect of H_s on BSD for air-water at U_g = 0.0167 m.s^{-1}

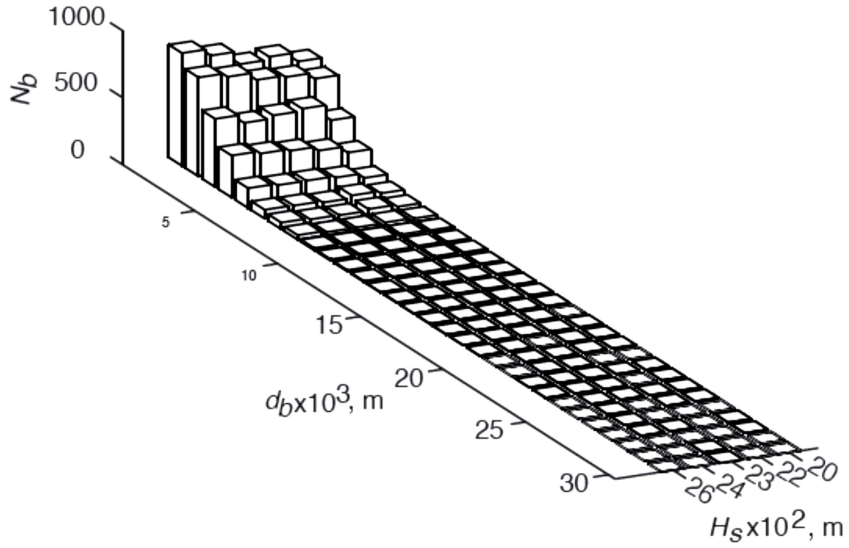

Figure 4.19: Effect of H_s on BSD for air-water at U_g = 0.0417 m.s^{-1}

4.3.2 BSD for Air-CMC solution

BSD for air-CMC solution was obtained at H_s=0.23 m. The BSD data is presented in Table A7 (Appendix-I).

BSD for 1.0 %(w/w) CMC solution at U_g = 0.0417 m.s^{-1} and H_s=0.23 m is presented in Figure 4.20. Number of bubbles decreases with increasing bubble diameter. It shows a single modal behaviour.

4.3.2.1 Effect of U_g

BSD for 1.0 wt % aq. solnution of CMC at H_s = 0.23 m, and for 0.008 m s^{-1} ≤ U_g ≤ 0.038 m.s^{-1} is presented in Figure 4.21. The number of small bubbles decreased with increasing U_g. The flow regime does not belong to category of bubbling flow regime as the bubbles are of not uniform size.

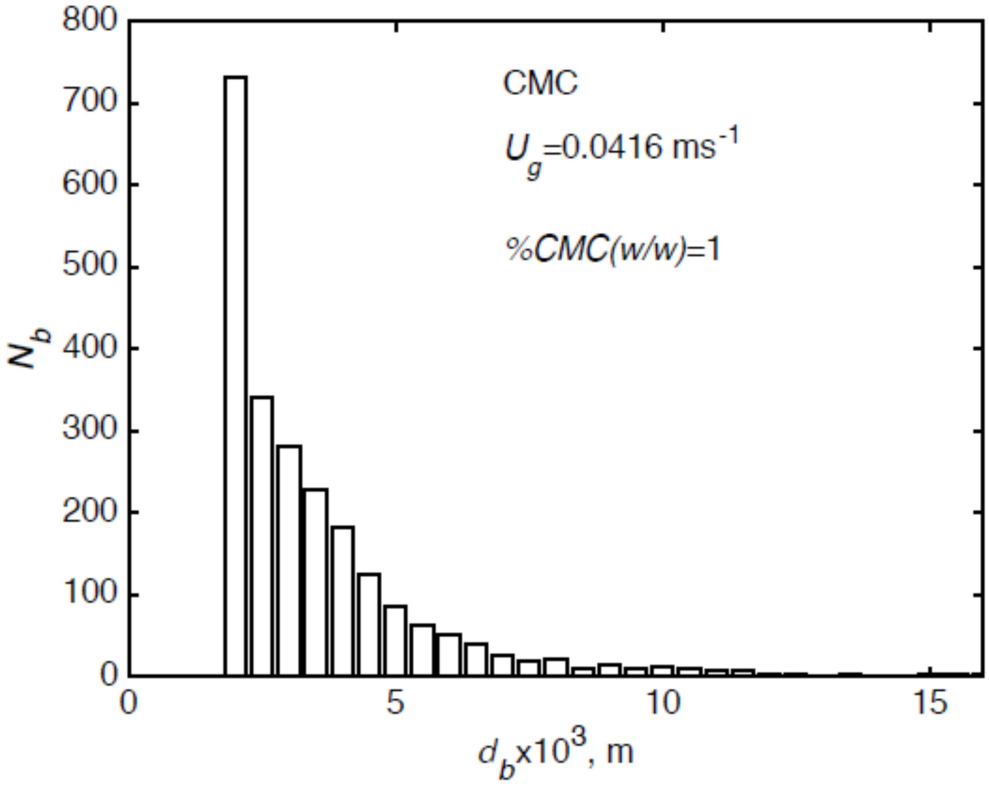

Figure 4.20: BSD for 1.0%(w/w) CMC solution at U_g = 0.0416 m.s^{-1}, H_s = 0.23 m.

4.3.2.2 Effect of Concentration: BSD for 0.1, 0.5 and 1.0 % (w/w) CMC in water and water (0%) at U_g=0.0375 m.s^{-1} and H_s=0.23 m is presented in Figure 4.22. Nature of the BSD is single model function. As the concentration increased the number of small bubbles increased.

From the trends observed it was observed that the BSD in all cases were single modal. Few large bubbles were also observed. Number of small bubbles increased with increasing value of static bed height in case of air-water systems and with concentration of CMC in the range of concentration from 0.0% to 3% (w/w)

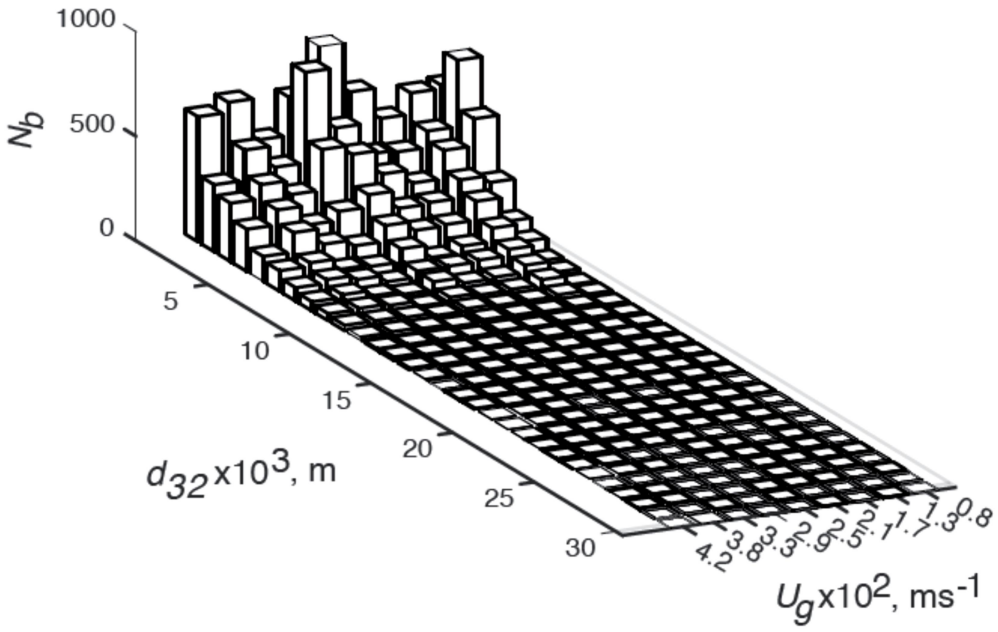

Figure 4.21. Effect of U_g on BSD for 1.0 % (w/w) CMC solution at H_s =0.23 m.

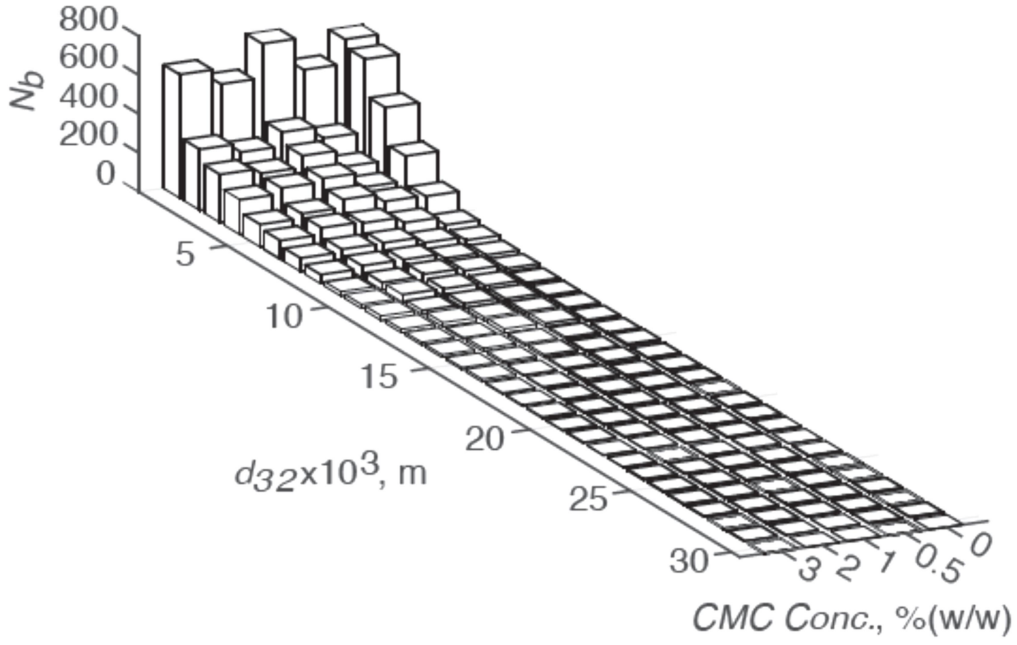

Figure 4.22. Effect of conc. on BSD for aq. CMC soln. at U_g=0.0375 m.s^{-1}, H_s=0.23 m.

4.4 Sauter-mean bubble diameter

From bubble size distribution, the value of d_{32} was calculated by

$$d_{32} = \sum_i d_i^3 \Big/ \sum_i d_i^2 \tag{4.8}$$

where d_i is projected area equivalent diameter of individual bubbles.

4.4.1 Air-distilled water system

Values of were evaluated at H_s in the range of 0.20 m to 0.28 m and for 0.008 m $s^{-1} \leq U_g \leq 0.058$ m.s^{-1} for air-distilled water.

4.4.1.1 Effect of H_s on d_{32}:

Variation of d_{32} as a function of U_g and H_s is presented in Figure 4.23. The values of d_{32} seem to be independent of H_s. Sauter mean diameter increases with increasing superficial gas velocity changes. The increase is less for U_g <0.04 m.s^{-1}. Above this value of U_g there is considerable increase of the value of d32 It indicates that above U_g =0.04 m.s^{-1} bubble coalescence starts taking place. This observation is in accordance to the drift flux plot (Figure4.13). Thus, it may be said that U_g =0.04 m.s^{-1} is the flow transition velocity.

Data of Cents et al (2005) for air-water system are also shown for comparison. There data also show that d_{32} increases with increasing U_g, however present data are about 100% higher than their data. Cents et al. (2005) used sintered porous plate as gas distributor. Therefore, the size of bubbles formed at the sparger in their studies could have been lower than that formed in the present studies.

Pohorecki et al. (1999) carried out numerical experiment and proposed the following equation for d_{32} after validating the equation for 7 organic solvents.

$$d_{32} = 0.289 \rho^{-0.552} \mu^{-0.048} \sigma^{0.442} U_g^{-0.124} \tag{4.9}$$

Present values are compared with that predicted using Equation 4.9 and presented in Figure 4.23. The predicted values of d_{32} are lower than present

experimental values of d_{32}. Equation 4.9 predicts bubble diameter to decrease with increasing superficial gas velocity. Similar trends were also reported by Millies and Mewas (1999) and Akita and Yoshida (1974). This trend is opposite to the present trend.

Experimental data for tap water measured by Al-Masry et al. [2006] are also shown in the figure. These values also are lower than the present values. It may be due to the fact that the hole diameter in the sparger in their study was 0.001 m which is lower than that used in the present study. In absence of bubble coalescence and bubble breakup the bubble diameter in the column will be close to that formed at the distributor.

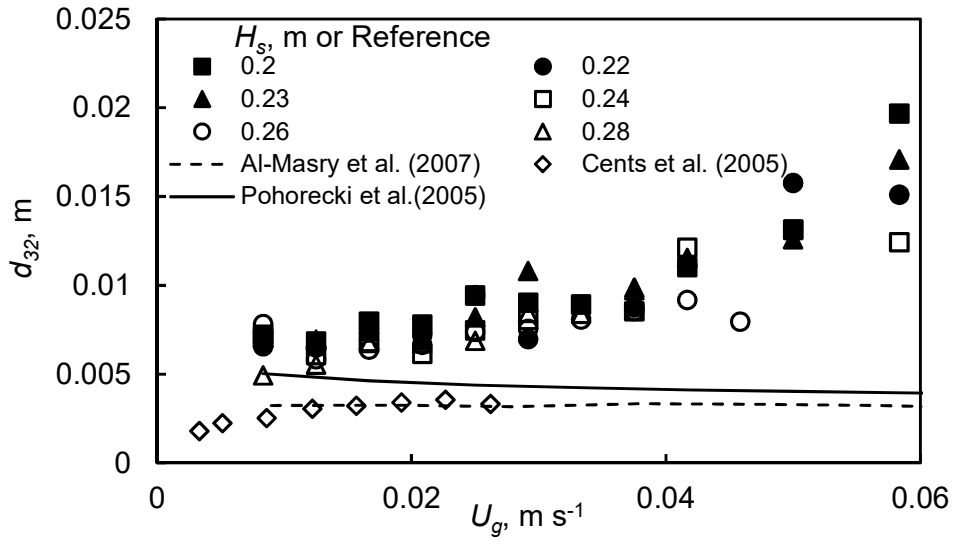

Figure 4.23: Variation of d_{32} as a function of U_g and H_s.

4.4.2 Air-CMC solution system

Variation of d_{32} as a function of U_g for H_s = 0.23 m and concentration of CMC = 0.1, 1.0, 2.0 and 3.0 % (w/w) is presented in Figure 4.25. The values of d_{32} increase with increasing U_g. Upto U_g < 0.03 m.s^{-1}, CMC concentration has little effect on the values of d_{32}. It may be attributed to the effect of formation of bubble indicating that liquid viscosity has no effect on d_{32}. At $U_g \geq 0.03$ m.s^{-1} there is large variation in values of d_{32}, however no definite trend was observed. There could be a change in the flow regime at U_g between 0.02 and 0.03 m.s^{-1}. It is in accordance of the drift flux in Figure 4.15 which also shows a change in flow regime at U_g = 0.03 m.s^{-1}.

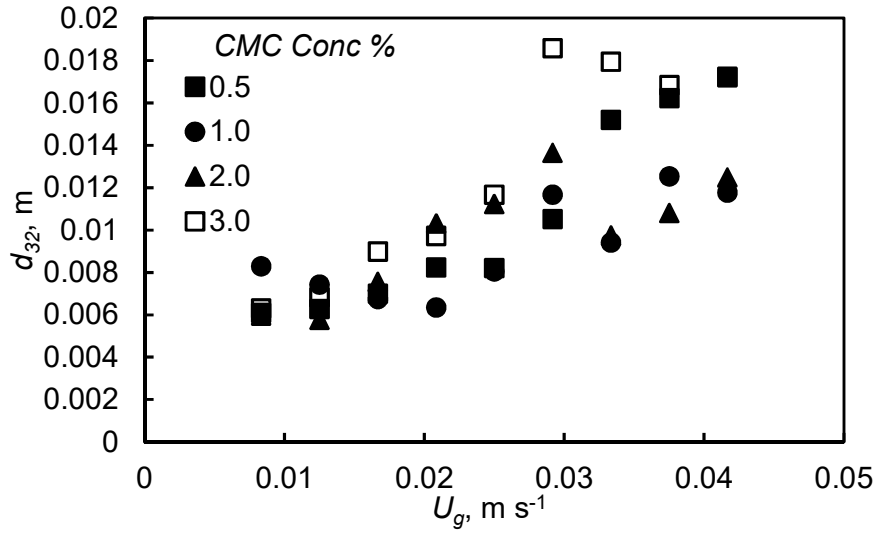

Figure 4.24: Variation of d_{32} with U_g at various CMC conc.

4.5 Aspect Ratio

Aspect ratio, E, is defined as a ration of minor axis to major axis. Its value is 1 for spherical particles and is less than 1 for other ellipsoids. The value of E for air-water system for U_g = 0.0083 m.s^{-1} and H_s = 0.20 m is presented in Figure 4.25. It is surprising to observe a wide variation in the values of E for even small bubbles. Besagni et al. (2016) also used image processing technique to determine the aspect ratio and observed somewhat similar results. It was thought to be due to distortion of the bubbles. It may also be due to overlapping of small bubbles. In case of large deviation in aspect ration the mean aspect ratio does not have any meaning and were not determined. Similar results were also observed for CMC solution of all concentrations.

4.6 Interfacial area

Specific interfacial area, a_i, in bubble columns has been investigated by several investigators. It is easily estimated from the value of d_{32}. The values of a_i were estimated using following equation.

$$a_i = 6\varepsilon / d_{32} \tag{4.10}$$

4.6.1 Effect of U_g and H_s on a_i for air-water system

Variation of a_i with U_g for static bed height, H_s = 0.20, 0.22, 0.23, 0.24, 0.26 and 0.28 m is presented in Figure 4.26. Value of a_i increases with increasing value of U_g and decreasing value of H_s. Experimental values of a_i reported by Cents et al. (2005) are also presented in the Figure. Present values of a_i are in close agreement to the data of Cents et al (2005) upto U_g =0.02 m.s^{-1}. Above this value of U_g, present values of a_i are lower than their values. Pohorecki et al. (1999) compared several correlations to predict the values of a_i and observed that a_i increases with increasing value of U_g. Following correlation for a_i was proposed.

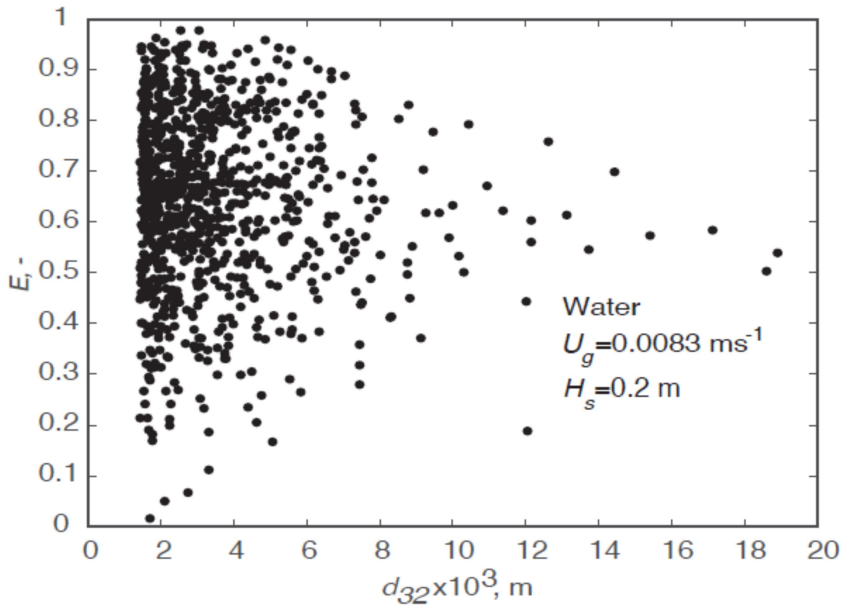

Figure 4.25: E for air/water at U_g=0.0083 m.s^{-1}, H_s=0.2 m.

$$a_i = 1120 U_g^{0.63} \tag{4.11}$$

Present data of a_i are about 50 % higher than that predicted from Equation 4.11. The trend of the data is very much similar to that observed by Pohorecki et al. (1999) and Cents et al. (2005).

4.6.2 Effect of U_g and CMC con. on a_i for air-CMC solution system

Values of a_i with U_g for CMC conc. = 0.5, 1.0, 2.0 and 3.0 % (w/w) are presented in Figure 4.27. Values of a_i for water increase with increasing value of U_g. Upto U_g < 0.017 m.s^{-1} there is large variation in values of a_i. The value of a_i increases with increasing CMC concentration. The value of a_i for 3.0% CMC is about 140% higher than that for 0.5% CMC solution. For U_g ≥ 0.017 m.s^{-1}, value of a_i for 3.0% CMC is about 70% higher than that for 0.5% CMC solution. The change in the nature of the dependence of a_i on CMC concentration at about U_g = 0.017 m.s^{-1} may be attributed to change in the flow regime.

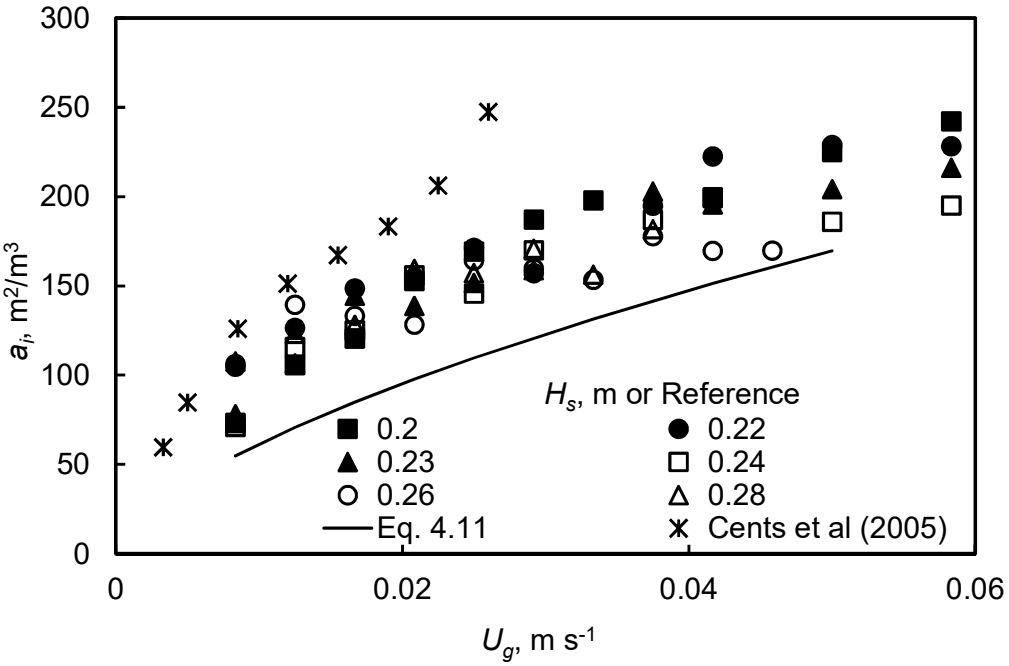

Figure 4.26: Variation of a_i with U_g and H_s for air-water system

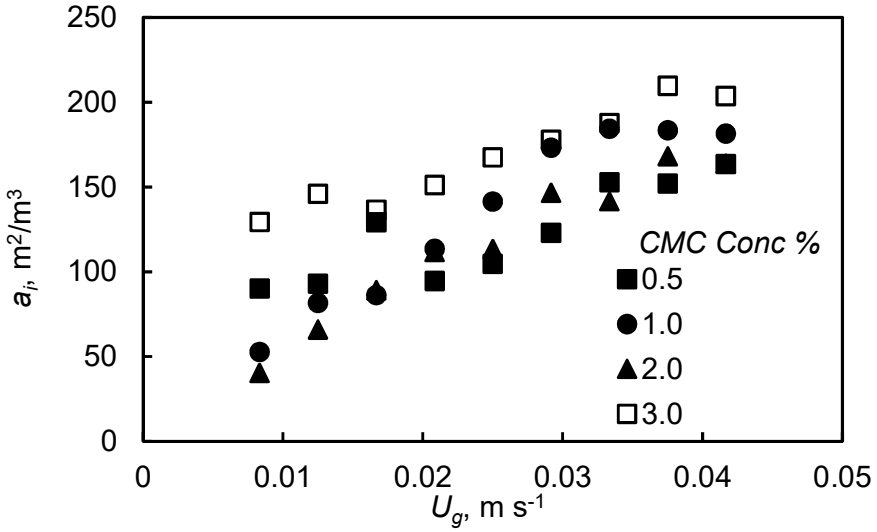

Figure 4.27: Variation of a_i with U_g and CMC concentration at H_s =0.23 m.

Thus, it is observed that photographic method can be used to measure the expanded bed height and foam layer thickness. It may be used to identify the entrance region. From the same images, through a suitable image processing algorithm, Sauter-mean bubble diameter, gas holdup and specific interfacial area can be estimated. The latter is closely related to volumetric mass transfer coefficient. A methodology to estimate ($k_L.a_i$) is presented below.

4.7 Volumetric Mass-Transfer Coefficient, ($k_L.a_i$)

Volumetric mass-transfer coefficient, ($k_L.a_i$), in bubbles columns has been studied by several investigators. The effect of fluid properties, column diameter and type of sparger has been investigated and correlations have been proposed. Some of the correlations are presented in Table 2.4. Few of these correlations are for ($k_L.a_i$) while several others have used Sherwood number, *Sh*. While k_L is dependent upon the hydrodynamics around the bubble, a_i depends upon the size of bubble, frequency of bubble formation and coalescence and breakup phenomena. Since the fluid motion in bubble column is induced by rising bubbles, the hydrodynamic conditions around bubble also depend upon the type of the sparger, column diameter and bubble size. The complex interdependence of these parameters makes it difficult to predict the value of ($k_L.a_i$) from fundamentals.

One of the approaches followed is measurement of value of a_i. The value of k_L can now be estimated from the experimental values of ($k_L.a_i$). Attempts can be made to estimate k_L from fundamentals. Due to good mixing, it has been thought to use Higbie's, surface renewal model to predict the value of k_L. Since, gas hold up and bubble diameter can be measured; value of k_L from a suitable model can be used to estimate ($k_L.a_i$). The difficulty in using Higbie's model is a suitable definition of critical time t_c.

4.7.1 A model for Volumetric Mass-Transfer Coefficient, ($k_L a_i$)

It has been shown that heat transfer in bubble columns can be explained by using the concept of isotropic turbulence [Deckwer (1980)]. The mass transfer between wall and bulk of the column is no different and an analogy between mass transfer and heat transfer exists [Verma (2002)]. Therefore, let us assume that mass transfer in a bubble column is also governed by turbulence. Higbie's surface renewal model (1935) may be used to predict the value of k_L. In this model, it is assumed that eddies arrive at the bubble surface, stay there for some time and then leave the bubble surface. During time of stay one dimensional unsteady state mass transfer takes place. Higbie's model gives the following expression for mass-transfer coefficient, k_L.

$$k_L = 2\sqrt{D_L/(\pi t_c)} \tag{4.12}$$

Here, D_L is diffusivity of the species transferred in the medium. However, difficulty in using Higbie's model is a suitable definition of critical time t_c. In Dankwert's model (1951), it is assume that probability of eddy leaving the surface is independent of age of the eddy at the surface. It is discarded as the turbulence is induced by bubbles and hence the critical time should always take into account the bubble properties.

Most of the bubbles have wake behind them. The shape of bubbles and length of their wakes are different. Let us assume that a spherical bubble with an equivalent diameter represent an average picture. The bubbles are moving up. When operated in a batch mode, the relative velocity of the bubble and liquid is equal to bubble velocity. It is assumed as a bubble move with a velocity, V_b, the fluid element at the upper tip comes into the contact of the bubble (Figure 4.28). It moves along the side of the bubble to a location where the lower half of the bubble starts. The fluid element leaves the bubble surface due to wake present in lower portion of the bubble. Thus, the fluid element travels a path, L, with a velocity V_b. During the stay the fluid element stays at

the bubble surface for a time, t_c. Mass transfer takes place by unsteady state diffusion into the fluid element. Higbie's expression for mass-transfer coefficient, k_L, given by Equation 4.12 can be used. The critical time, t_c, which is time taken by the fluid element to travel on the surface of the bubble, can be written in terms of path and velocity of the fluid element.

$$t_c = L/V_b \tag{4.13}$$

An expression for swarm velocity, V_b, given by Krishna et al. (1999) is used.

$$V_b = V_b^0 \left(1-\varepsilon\right)^{n-1} \tag{4.14}$$

For air-water system n=2. The value of V_b^0 is given by

$$V_b^0 = 1.53\left(\sigma g/\rho_L\right)^{0.25} \tag{4.15}$$

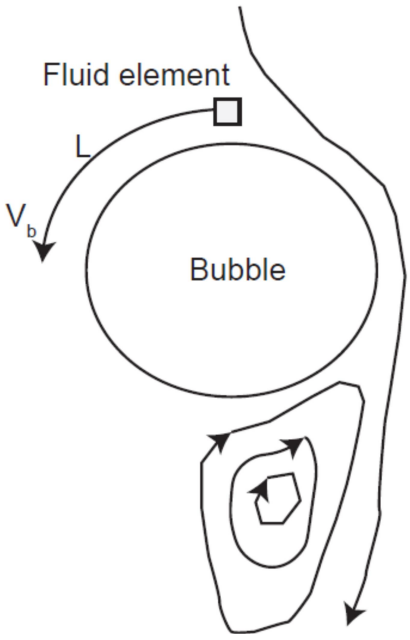

Figure 4.28: Schematic sketch of the model

On the downside of the bubble there is a wake. Let us assume that the wake is closed. As a result the fluid on downside of the bubble is saturated and no significant

mass transfer takes place. Thus the path of the fluid element, L, in terms of the bubble diameter is given by

$$L = \pi d_b / 2 \tag{4.16}$$

To estimate the value of ($k_L.a_i$), value of a_i is required. Though, experimental values of a_i may be used, the following methodology for its estimation was used. Gas hold up was estimated using following correlation of Akita and Yoshida (1973).

$$\varepsilon/(1-\varepsilon)^4 = 0.20 Bo^{1/8} Ga^{1/12} Fr \tag{4.17}$$

Akita and Yoshida (1974) has proposed following correlation to estimate Sauter mean bubble diamter. The same is used to represent equivalent bubble diamter, d_b.

$$d_{32}/D = 26 Bo^{-0.5} Ga^{-0.12} Fr^{-0.12} \tag{4.18}$$

Total number of bubbles, n_b, per unit volume is estimated as

$$n_b = \varepsilon/\left(\pi d_b^2/6\right) \tag{4.19}$$

The specific interfacial area per unit volume can be estimated as

$$a_i = n_b\left(\pi d_b^2\right) \tag{4.20}$$

Values of k_L were estimated by using Equations 4.12-4.20. These values were compared with values obtained three others procedures. Estimation of *Sh* requires values of ε and d_b. Though several options are available only three methodologies as discussed below were chosen for comparion.

4.7.2 Estimation of ($k_L.a_i$) using Correlations by Akita and Yoshida (1974)

Akita and Yoshida (1974) carried out extensive work and proposed all necessary correlations. The values of ε and d_b were estimated using Equations 4.17 and 4,18 respectively. These were used in the following correlation to estimate Sherwood number, *Sh*, [Akita and Yoshida (1974)].

$$Sh = \left(k_L d_{32} / D_L\right) = 0.5 Sc^{1/2} Bo^{3/8} Ga^{1/4} \varepsilon^{1.1} \quad (4.21)$$

The value of k_L can now be estimated. The values of a_i were estimated using following correlation by Akita and Yoshida (1974).

$$a_i D = \left(1/3\right) Bo^{0.5} Ga^{0.1} \varepsilon^{1.13} \quad (4.22)$$

Value of ($k_L.a_i$) can be obtained by multiplying the valus of k_L and a_i.

4.7.3 Estimation of ($k_L.a_i$) using Correlations by Pohorecki et al. (2001)

Pohorecki et al. (2001) proposed following correlation for a_i, d_{32} and ε.

$$a_i = 0.26\left(\rho_L g U_G\right)^{0.63} \quad (4.23)$$

$$d_{32} = 1.658 \times 10^{-3} U_g^{-0.12} \quad (4.24)$$

$$\varepsilon_G = 0.383 U_g^{0.65} \sigma^{-0.52} \quad (4.25)$$

Since no correlation for mass-transfer coefficient was proposed by them, the following correlation by Diaz et al. (2009) was used to estimate Sherwood number.

$$Sh = 0.67 \mathrm{Re}^{0.6} Sc^{0.5} \quad (4.26)$$

The value of k_L was estimated from Sherwood number and the value of ($k_L.a_i$) was estimated by multiplying the values of k_L and a_i.

4.7.4 Estimation of ($k_L.a_i$) using Correlations by Pohorecki et al. (2005)

Pohorecki et al (2005) proposed the following correlation for d_{32}. The value of a_i was estimated considering the bubbles to be of spherical shape.

$$d_{32} = 0.289 \rho^{-0.552} \mu^{-0.048} \sigma^{0.442} U_g^{-0.124} \quad (4.27)$$

The method of estimation of k_L was same as the previous method in section 4.3 except that a new correlation for a_i was used.

The values of k_L by all the four methods were compared for air-water system in Figure 4.29. The present method and the method using correlations of Akita and

Yoshida (1974) compared well. One striking feature is that the value of k_L is almost independent of U_g. Two other methods based on correlations of Pohorechi et al (2001, 2005) are very high. The method using correlation of Pohorecki et al (2001) predicts decrease of k_L with increasing superficial gas velocity.

To understand the reason for such a wide variation the values of estimated in these cases the values of a_i were compared in Figure 4.30. It may be seen that these is a wide variation of a_i. The values of a_i were estimated using correlations of Akita and Yoshida (1974) given by Equation 4.22 and present methods are close to each other.

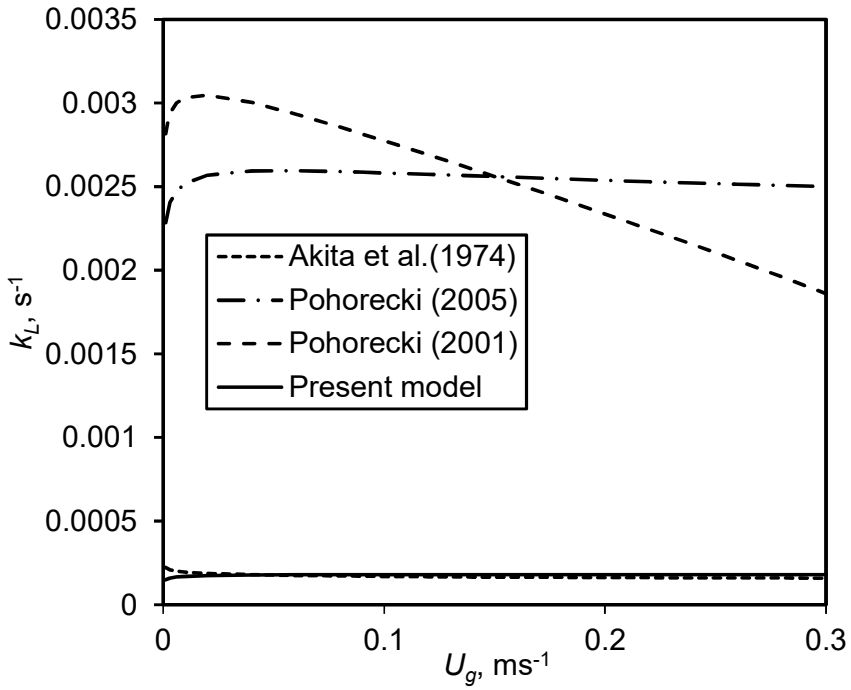

Figure 4.29: Comparison of k_L estimated by present method with that using correlations of Akita et al(1974), Pohorecki (2001) and Pohorecki (2001).

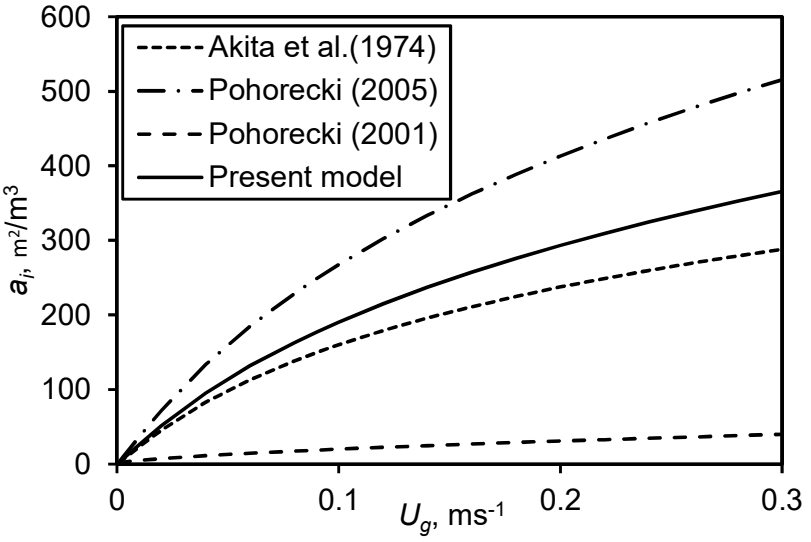

Figure 4.30: Comparison of a_i estimated by present method with that using correlations of Akita et al(1974), Pohorecki (2001) and Pohorecki (2001).

It may be said that Higbie's model may be used to estimate the value of k_L. However, it requires the bubble diameter and bubble velocity to predict the value t_c, Both are measurable using image photographic method. A striking feature observed is that the value of k_L is independent of U_g. Hence, a constant value of k_L may be chosen. By measuring the value of a_i, values of ($k_L.a_i$) may be estimated.

Estimated values of ($k_L.a_i$) estimated, using the estimated values of k_L and a_i are compared in Figure 4.31. The method using correlation of Pohorecki et al. (2005) predicted very high values of ($k_L.a_i$). Excluding this method, values of ($k_L.a_i$) estimated by other three methods are presented in Figure 4.32. They all show similar trend. The present method is about 50% lower than that predicted by procedure based on correlations of Pohorecki et al. (2001) and 50% higher than that predicted by procedure based on correlations of Akita and Yoshida (1974). By taking a constant value of k_L it is still possible to estimate ($k_L.a_i$).

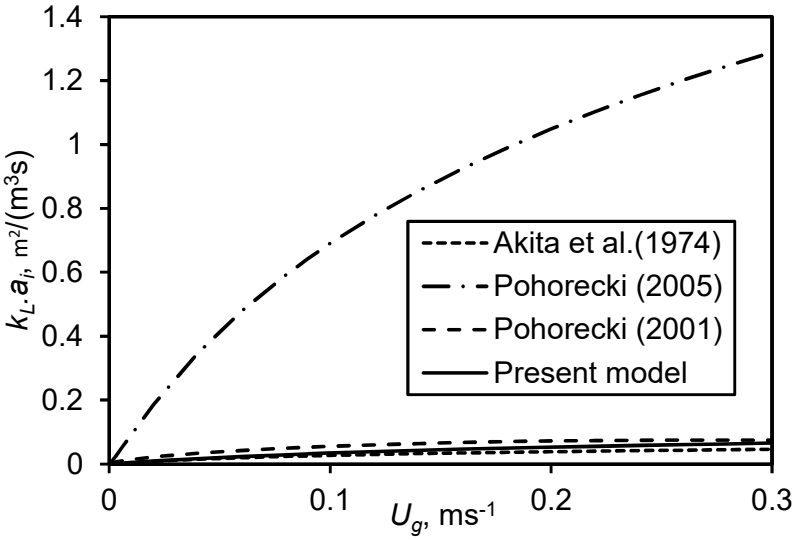

Figure 4.31: Comparison of ($k_L.a_i$) estimated by present method with that using correlations of Akita et al(1974), Pohorecki (2001) and Pohorecki (2001).

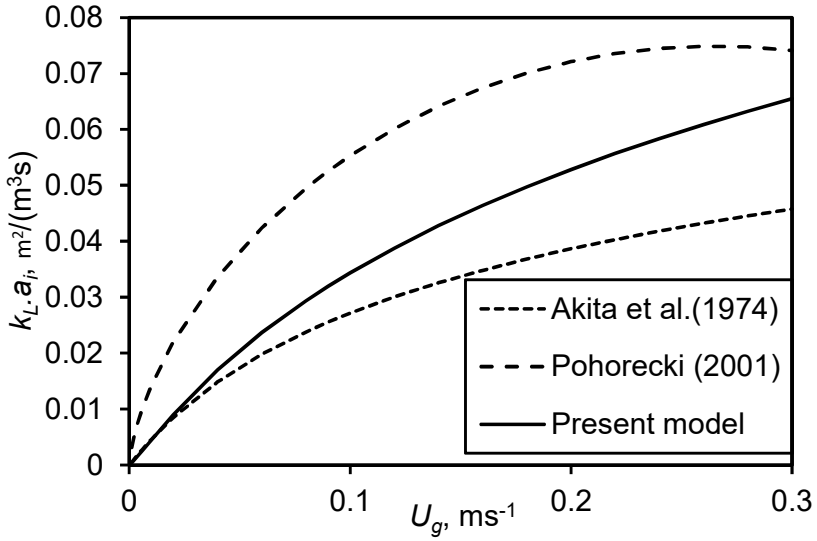

Figure 4.32: Comparison of ($k_L.a_i$) estimated by present method with that using correlations of Akita et al(1974), Pohorecki (2001) and Pohorecki (2001).

In several applications involving biomaterials and polymers the liquid is non-Newtonian. Most of correlations for gas holdup, bubble behavior and transfer coefficients are applicable to Newtonian fluids only. In case fluid is non-Newtonian these correlations are used by replacing viscosity by apparent viscosity. There are few methods to estimate shear rate and apparent viscosity for non-Newtonian fluids in bubble columns. However, they are applicable to power law fluids only. In bioprocessing applications other rheological models are frequently used. Hence, there is a need for a rational method to evaluate the apparent viscosity for rheological models other than power law fluid. A simple model for the estimation of shear rate and apparent viscosity of non-Newtonian fluids in bubble columns is proposed in the following section.

4.8 MODEL FOR APPARENT VISCOSITY

The net movement of bubbles is in upward direction. Though radial (or horizontal) velocity component of bubbles may also be present, it is being ignored since the vertical velocity component is generally much larger than horizontal velocity component. Following assumptions have been made to arrive at a simplified picture of bubble motion and fluid flow.

(i) Only vertical component of bubble velocity is present. The horizontal component of velocity is absent. Thus, it is same as bubble velocity, U_b.

(ii) The bubble locations are such that they may be considered to move into various planes separated by inter-bubble distance, L_b, as shown in Figure 4.33. This distance may be determined from gas holdup in the column.

(iii) The liquid present in the plane containing bubbles also move with the velocity, U_b, same as that of the bubbles.

(iv) Liquid velocity at a vertical plane in the middle of two adjacent vertical layers of bubbles is assumed to be zero (Figure 4.33). This assumption indicates a net movement of the liquid upwards, which may be neglected only when gas holdup is small.

(v) All bubbles are of same diameter, which is true when bubble coalescence is absent.

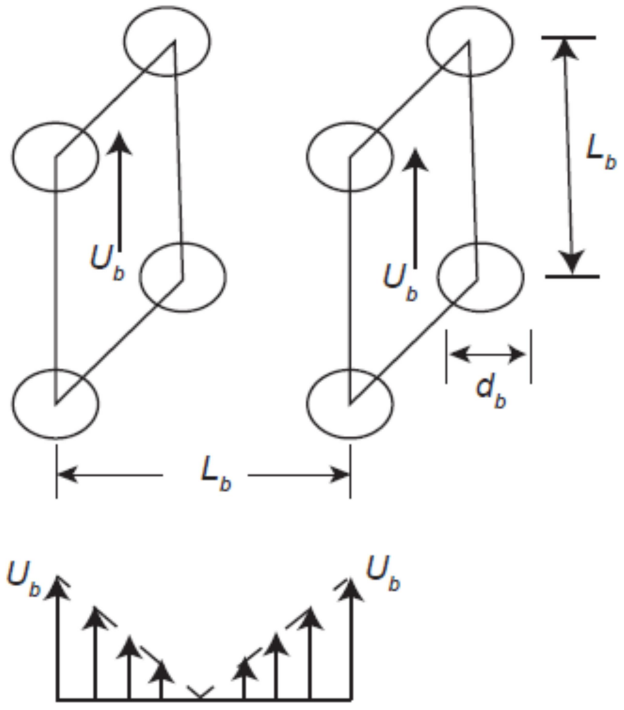

Figure 4.33: Average bubble position and velocity assumed in a bubble column

The average shear rate depends upon the flow conditions prevailed in the bubble column. With the above assumptions the flow conditions are analogous to a plane moving parallel to a flat imaginary stagnant fluid-wall at midpoint of bubble layers. The velocity gradient is assumed to be linear in case of Newtonian fluids. It is boldly assumed that velocity gradient is linear for non-Newtonian fluids also. This consideration allows us to develop a simple procedure to estimate shear stress for several rheological models.

The relationship between bubble velocity, U_b, and average inter-bubble distance, L_b depends upon the arrangement of bubbles. Let us assume cubic arrangement of average position of bubbles. It can be shown that for average position of the bubbles of uniform size, d_b, the value of L_b can be written as.

$$L_b / d_b = \left(\varepsilon / \varepsilon_m\right)^{1/3} \tag{4.28}$$

Here, ε and ε_m are gas holdup and maximum gas holdup for tightly packed bubbles respectively.

It is common to use apparent viscosity in place of viscosity in correlations developed for Newtonian fluids. Apparent viscosity is defined as ratio of shear stress and shear rate.

$$\mu_0 = \tau_{yx} / \dot{\gamma} = \tau_{yx} / \left|dv_x / dy\right| \tag{4.29}$$

For linear velocity profile between a layer of bubbles and midpoint of two adjacent layers, the shear rate can be obtained easily written as.

$$\dot{\gamma} = dv_x / dy = U_b / (L/2) = \left(U / \varepsilon\right)\left(\varepsilon_m / \varepsilon\right)^{1/3}\left(2 / d_b\right) \tag{4.30}$$

Equation 4.30 based on the present model to estimate shear rate is valid for all rheological models. The proposed model requires values of gas holdup, bubble diameter and rheological parameters. Application of the model will be illustrated developing gas hold correlation for power law fluid.

4.9 Gas holdup Correlation for Power Law Fluid

The experimental data for ε and d_b for water and glucose as Newtonian and aqueous solutions of CMC, Boger and Xanthan gum as non-Newtonian fluids are reported by Esmaeili et al. (2015). Values of ε and bubble chord length were obtained by using digitizer program. The values of d_b were taken as 1.5 times bubble chord length. The procedure for development of correlation is as following.

For cubic arrangement of bubbles ε_m=0.5236. At a given value of U_g, value of L_b was estimated from Equation 4.28. Column diameter, D=0.292 m. Value of μ_0 was evaluated from the expression given in Table 2.5 for power law fluid. Froude number, Fr, and Morton number, Mo, were estimated by the following equations

$$Fr = U_g \Big/ \sqrt{gD} \tag{4.31}$$

$$Mo = (g\mu_0^4)\big/(\rho\sigma^3) \tag{4.32}$$

A total of 174 data points for all systems were fitted using 'Solver' addin of 'Excel' to give the following correlations.

$$\varepsilon = 9.23 Mo^{0.034} Fr^{0.91} \qquad U_g \le 0.1 \text{ m.s}^{-1} \tag{4.33}$$

$$\varepsilon = 9.5 Mo^{0.038} Fr^{0.54} \qquad U_g > 0.1 \text{ m.s}^{-1} \tag{4.34}$$

Values of ε estimated from Equations 4.33 and 4.34 are compared with experimental values of by Esmaeili et al. (2015) in Figure 4.34. Most of the predicted values were within 20% of experimental values. No systematic deviation is visible in the parity plot. It may be noted that the exponent of Fr changes at U_g = 0.1 m.s^{-1} indicating different flow regimes. At high values of U_g (or ε) the deviation is less irrespective of the fluid used. It may be possible that there are not enough bubbles to justify the assumptions at low values of U_g.

The methodology may be applied not only to power law fluids but also to other rheological models. The model can be used to fit correlations for data available for different rheological models. It can also be used for simulation studies involving correlations developed for Newtonian fluids also.

In brief a methodology to predict volumetric mass-transfer coefficient using experimental data from images of bubble column is presented. A model is also proposed to extend the model for non-Newtonian fluids by using apparent viscosity.

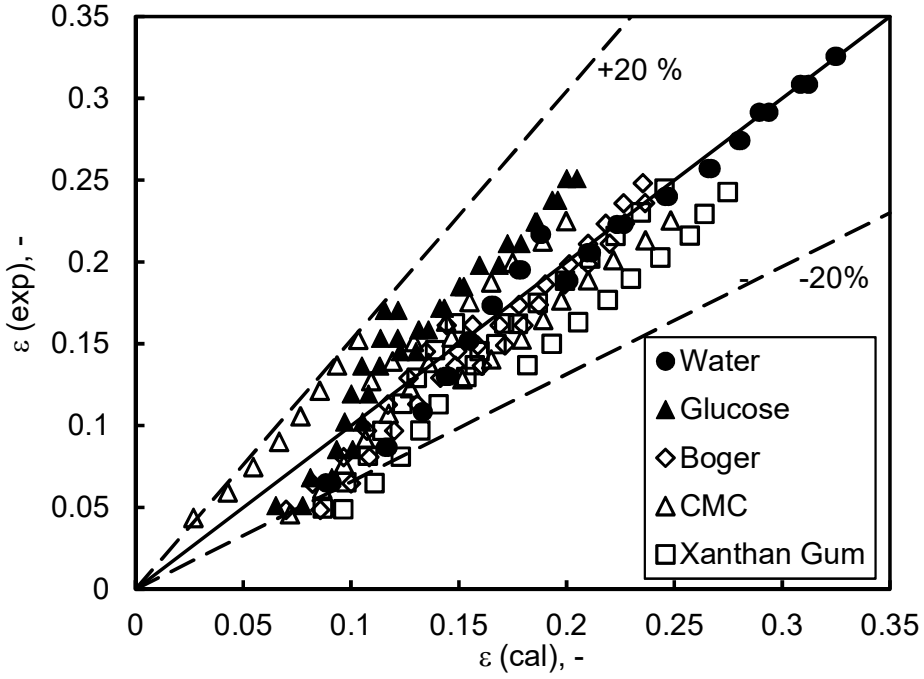

Figure 4.34: Comparison of values of gas holdup estimated from Equations 4.33 and 4.34 with data of Esmaeili et al. (2015).